電気学会論文誌●（●●●●●●●部門誌）
IEEJ Transactions on ●●●●●●●●●●●●●●●●
Vol.●● No.● pp.●-●● DOI: ●.●●/ieejeiss.●●.●

Paper

A 22kW Three-phase Wireless Power Transfer System in Compliance with CISPR 11 and ICNIRP 2010

Keisuke Kusaka[a)*] Member, Rintaro Kusui[*] Student-member,
Jun-ichi Itoh[*] Senior-member, Daisuke Sato[**] Member, Tetsu Shijo[***] Non-member,
Shuichi Obayashi[***] Non-member, Masaaki Ishida[***] Non-member

(Manuscript received Jan. 00, 20XX, revised May 00, 20XX)

Techniques to reduce electromagnetic emission in high-power wireless power transfer (WPT) systems are required because the radiated emission of the WPT must comply with the regulation published by CISPR (International Special Committee on Radio Interference) and ICNIRP (International Commission on Non-ionizing Radiation Protection.) In this paper, a three-phase WPT system, which complies with CISPR 11, group 2, class A is developed. The three-phase WPT system has six solenoid coils on the primary side and six solenoid coils on the secondary side. The use of 12 coils allows radiation noise reduction as the radiation noise is emitted to the opposite direction of the pairs of coils. Moreover, the cross-coupling among six coils on the common side is canceled by adjusting the position of coils. The electromagnetic compatibility of the 22kW prototype is evaluated in a 10 m anechoic chamber according to the CISPR 11 guideline. The prototype fully complies with CISPR 11, class A, group 2 with respect to electromagnetic emission. Moreover, it also complies with ICNIRP guidelines in 2010 at a distance of 340 mm or more from the edge of the coils.

Keywords : Electromagnetic compatibility, Electromagnetic induction, Inductive power transmission, wireless power transmission

1. Introduction

The sales volume of electric vehicles (EVs) has been slowly increasing in this decade due to global warming and environmental issues. One of the reasons that are hindering the rapid adoption of EVs is their short travel distance. Since users of EVs are frequently required to charge onboard batteries, they are not still substituted for conventional vehicles. As one of the solutions to improve the convenience of EV users, wireless power transfer (WPT) with magnetic induction has been actively studied in this decade[(1–8)].

In the international standardization for the WPT system by ISO/IEC, the WPT systems are classified into five classes (WPT1–5) based on the input power[(9)]. The largest class is WPT5, with an input power of 22 kW or more. One of the specific difficulties of high-power WPT is electromagnetic compatibility (EMC). An increase in the transmission power exposes EMC problems due to the radiated emission because the WPT system transmits power using magnetic coupling. The electromagnetic emission may cause interference with radio communications, malfunction of electrical equipment, or harm to human bodies. In order to ensure that the WPT system does not affect equipment or the human body, the electromagnetic radiation from the WPT system must comply with the guidelines published by ICNIRP and CISPR. The guideline published by ICNIRP focuses on the effect on human bodies. In contrast, the guidelines by CISPR focuses on the effect on the interference with radio communications and malfunction of electrical equipment. The high-power WPT system must comply with both regulations.

For WPT5, high-power wireless power transfer systems have been developed[(10–16)]. In (11–13), the WPT systems with an input power of 22 to 50 kW have been reported. However, the radiated emission test has not been mentioned in the literature. In (14–15), only the magnetic field near WPT systems has been evaluated to compare with ICNIRP guidelines. The compatibility with the CISPR guidelines has not been discussed; nevertheless, the radiation noise from WPT systems may interfere with the radio communications. The two-channel 44-kW WPT system is demonstrated in (16). The radiated emission at 10 m from the WPT system is evaluated in an anechoic chamber for the compatibility test with the regulation in Japan. However, the compatibility with the CISPR guidelines has not been discussed in this paper. Nevertheless, compliance with both guidelines is essential to put the high-power WPT system into practical use.

In this paper, the 22-kW three-phase WPT system (WPT5) is developed. The developed 22-kW system reduced the radiative emission using multiple coils. Moreover, the cross-coupling effect by the multiple coils is cancelled using three-phase transmission and coil structure. It is demonstrated that the 22-kW prototype satisfies CISPR 11, class A, group 2 published in 2009, and guideline for general public exposure published by ICNIRP in 2010.

a) Correspondence to: Keisuke Kusaka. E-mail: kusaka@vos.nagaokaut.ac.jp
* Nagaoka University of Technology
1603-1, Kamitomioka, Nagaoka, Niigata 940-2188, Japan
** Nagaoka Motor Development Co., Ltd.,
2085-16, Fukasawa, Nagaoka, Niigata 940-2135, Japan
*** Toshiba Corporation
1, Komukai-Toshiba-cho, Saiwai-ku, Kawasaki, Kanagawa 212-8582, Japan

2. Three-phase WPT System with EMI Reduction Capability

2.1 Circuit Configuration Figure 1 shows the three-phase WPT system. The WPT system has six solenoid-type transmission coils for the primary side and six coils for the secondary side. The positions of six coils for the primary and secondary side are fixed, respectively, as shown in Fig. 1 (a). The primary and secondary sides are connected in star winding for three-phase transmission. Note that the delta-delta, star-delta, or delta-star windings can be used for the system, whereas the star-star windings are used in this paper. The six coils are used for each of the primary and secondary sides to reduce the effect of the cross-coupling among the coils. In conventional three-phase WPT systems[17–19], the circulating current due to the cross-coupling among the primary coils or secondary coils degrades the transmission efficiency. The WPT system has the reduced effect of cross-coupling by optimizing the positional relationship and figures of the six coils, as explained in the next section.

In the proposed system, only the magnetic couplings M between the paired coils such as L_{u1A} and L_{u2A} contribute to supplying power from the primary side to the secondary side. Other couplings, typically called cross-coupling, cause the unintended induced voltage on each coil. In WPT systems with multiple transmission coils, the induced voltage alternates by the current on the other coil. The unintended induced voltage is not compensated by the resonant capacitors. In other words, the other magnetic couplings should be zero for the power transmission with a unity power factor.

The three-phase inverter is used on the primary side. The inverter is operated with a square wave output voltage. On the secondary side, the diode bridge rectifier is used. The resonant capacitors C_{u1}, C_{v1}, and C_{w1} are connected to the output of the inverter for the compensation of a weak magnetic coupling M. Consequently, the resonant capacitors C_{u2}, C_{v2}, and C_{w2} are connected into the input of the three-phase diode bridge rectifier for the compensation. The inverter is operated in a zero-voltage switching (ZVS) condition by operating the inverter with a slightly higher frequency than the resonant frequency owing to the series resonance. In the ZVS condition, the switching loss of MOSFETs is reduced because a parasitic capacitor is discharged before them switching due to the circulating current during the deadtime[20].

2.2 Radiation Noise Reduction Figure 2 is a schematic of the primary and secondary coils. The key technique to reduce the radiation noise is the six pairs of solenoid coils placed in the opposite. The series-connected two coils on the common phase are magnetically differential. Because the amplitude of the current on each coil and the direction of the magnetic flux is in the opposite direction, radiation noise measured at 10 m from the center of coils is suppressed[16]. Note that the measurement distance is

provided by the guideline for radiation noise such as CISPR.

Moreover, the proposed system has six coils for three-phase transmission. The transmission coils are placed every 60 degrees. In the conventional three-phase WPT system, the cross-coupling cannot be ignored because the cross-coupling degrades the transmission efficiency because of the circulating current on the primary side or the secondary side. In the proposed system, the effect of cross-coupling M_{an}, M_{bn}, M_{cn}, M_{a12}, M_{b12}, or M_{c12} (n = 1 or 2) is reduced to approximately zero, as explained in the next section.

Figure 3 compares the magnetic field analyzed by an electromagnetic analysis (JSOL Corp., JMAG) between the three-phase WPT system with six coils and the proposed WPT system with 12 coils. In the three-phase WPT system with six coils, the

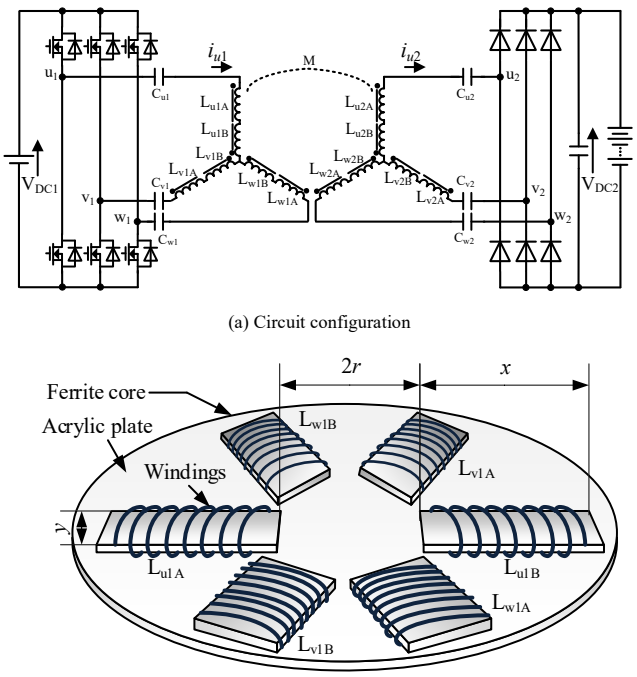

Fig. 1. Three-phase wireless power trasnfer system with 12 coils. The two coils connected in series is differentially connected for radiation noise reduction. The secondary coils is the same to the primary coils except the number of turns.

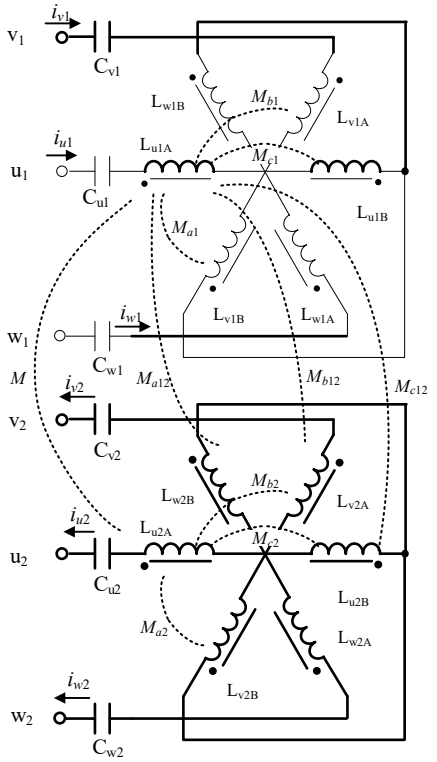

Fig. 2. Transmission coils and magnetic couplings among 12 coils. The magnetic couplings except the main couplings M do not contribute transmitting power.

$$\begin{pmatrix} v_{u1A} \\ v_{u1B} \\ v_{v1A} \\ v_{v1B} \\ v_{w1A} \\ v_{w1B} \\ v_{u2A} \\ v_{u2B} \\ v_{v2A} \\ v_{v2B} \\ v_{w2A} \\ v_{w2B} \end{pmatrix} = \begin{pmatrix} L_{1Ys} & M_{c1} & M_{b1} & M_{a1} & M_{b1} & M_{a1} & M & M_{c12} & M_{b12} & M_{a12} & M_{b12} & M_{a12} \\ M_{c1} & L_{1Ys} & M_{a1} & M_{b1} & M_{a1} & M_{b1} & M_{c12} & M & M_{a12} & M_{b12} & M_{a12} & M_{b12} \\ M_{b1} & M_{a1} & L_{1Ys} & M_{c1} & M_{b1} & M_{a1} & M_{b12} & M_{a12} & M & M_{c12} & M_{b12} & M_{a12} \\ M_{a1} & M_{b1} & M_{c1} & L_{1Ys} & M_{a1} & M_{b1} & M_{a12} & M_{b12} & M_{c12} & M & M_{a12} & M_{b12} \\ M_{b1} & M_{a1} & M_{b1} & M_{a1} & L_{1Ys} & M_{c1} & M_{b12} & M_{a12} & M_{b12} & M_{a12} & M & M_{c12} \\ M_{a1} & M_{b1} & M_{a1} & M_{b1} & M_{c1} & L_{1Ys} & M_{a12} & M_{b12} & M_{a12} & M_{b12} & M_{c12} & M \\ M & M_{c12} & M_{b12} & M_{a12} & M_{b12} & M_{a12} & L_{2Ys} & M_{c2} & M_{b2} & M_{a2} & M_{b2} & M_{a2} \\ M_{c12} & M & M_{a12} & M_{b12} & M_{a12} & M_{b12} & M_{c2} & L_{2Ys} & M_{a2} & M_{b2} & M_{a2} & M_{b2} \\ M_{b12} & M_{a12} & M & M_{c12} & M_{b12} & M_{a12} & M_{b2} & M_{a2} & L_{2Ys} & M_{c2} & M_{b2} & M_{a2} \\ M_{a12} & M_{b12} & M_{c12} & M & M_{a12} & M_{b12} & M_{a2} & M_{b2} & M_{c2} & L_{2Ys} & M_{a2} & M_{b2} \\ M_{b12} & M_{a12} & M_{b12} & M_{a12} & M & M_{c12} & M_{b2} & M_{a2} & M_{b2} & M_{a2} & L_{2Ys} & M_{c2} \\ M_{a12} & M_{b12} & M_{a12} & M_{b12} & M_{c12} & M & M_{a2} & M_{b2} & M_{a2} & M_{b2} & M_{c2} & L_{2Ys} \end{pmatrix} \frac{d}{dt} \begin{pmatrix} i_{u1} \\ -i_{u1} \\ i_{v1} \\ -i_{v1} \\ i_{w1} \\ -i_{w1} \\ i_{u2} \\ -i_{u2} \\ i_{v2} \\ -i_{v2} \\ i_{w2} \\ -i_{w2} \end{pmatrix} \quad \cdots\cdots(1)$$

coils L_{u1B}, L_{v1B}, L_{w1B}, L_{u2B}, L_{v2B}, and L_{w2B} are removed from the system with 12 coils. In this analysis, a current with a frequency of 85 kHz is provided into each winding. The primary and the secondary current are 28 and 46 A, respectively. The magnetic field strength at 10 m from the center of the coil has been compared. The proposed WPT system has approximately the same magnetic field as the conventional WPT near the coils because the distance between the two magnetomotive forces is relatively far apart compared to the measurement distance. The proposed WPT system with 12 coils has a lower magnetic flux density than the conventional WPT system away from the center of the coils. Note that the radiation noise from the WPT system is measured and evaluated at 10 m in the CISPR 11 guidelines.

2.3 Reduction in Effect of Cross-coupling The WPT system with multiple coils on the primary side or the secondary side has a critical problem that the transmission coils have cross-coupling, which is also called cross-coupling" among the coils[16, 21–22]. In (22), it is reported that the analytical results of efficiency and voltage transfer ratio of the three-phase WPT system has an error to the experimental results due to the cross-coupling. The circulating current causes a decrease in transmission efficiency.

In this paper, the effect of cross-coupling is reduced to approximately zero by six coils, which are circularly placed, and a three-phase current on the six coils. Here, the reduction method is explained, focusing on L_{u1A} in Fig. 2. The cross-coupling on the primary side for L_{u1A} is from others on the primary side L_{u1B}, L_{v1A}, L_{v1B}, L_{w1A}, and L_{w1B}. Note that the types of cross-coupling are limited to three types, M_{a1}, M_{b1}, and M_{c1}, by placing the coils in a circle. The sum of the magnetic flux from these coils on L_{u1A} is zero by designing the figures of coils, such as the radius of six coils, the width, and the length of each coil.

The reduction method of the interference is described using the induced voltage on L_{u1A} in this section. Equation (1) presents the induced voltage on the 12 coils. The variables M is the main coupling for power transmission, M_{an}, M_{bn}, M_{cn}, M_{a12}, M_{b12}, and M_{c12} are the cross-coupling, L_{nYs} is the self-inductance of each coil. Here, the cross-coupling M_{a12}, M_{b12}, M_{c12} can be ignored because the different heights and the different directions of the solenoid coils cause significant small coupling. Note that the effect of cross-coupling M_{a12}, M_{b12}, M_{c12} is also canceled by the design of transmission coils, although it can be ignored in this paper.

From the first line of (1), the induced voltage of the coil L_{u1A} is expressed by

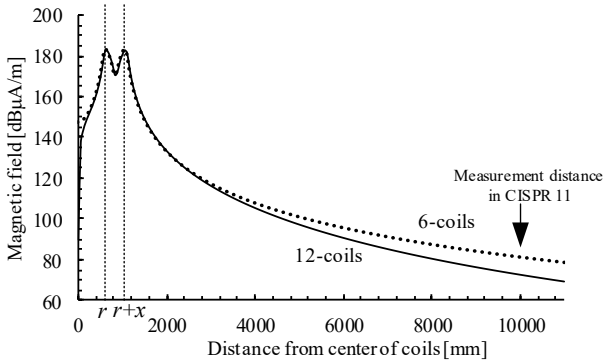

Fig. 3. Comparison in magnetic field strength between the six-coils WPT and proposed 12-coils WPT.

$$v_{u1A} \approx L_{1Ys}\frac{di_{u1}}{dt} + M\frac{di_{u2}}{dt} - M_{a1}\left(\frac{di_{v1}}{dt} + \frac{di_{w1}}{dt}\right) + M_{b1}\left(\frac{di_{v1}}{dt} + \frac{di_{w1}}{dt}\right) - M_{c1}\frac{di_{u1}}{dt} \quad \cdots\cdots(2).$$

As shown in (2), the terms on the first line represent the induced voltage by the self-inductance and the mutual inductance, which contributes to transmitting power to the secondary side. The terms on the second line are from the interferences. The induced voltage by the interferences M_{a1}, M_{b1}, and M_{c1} does not transmit power to the secondary side. On the contrary, the third to fifth terms cause the circulating current. The sum of these terms must be zero. Adjusting the sum of the third to fifth to zero using the three-phase transmission characteristic reduces the effect of the cross-coupling. The three-phase current is an equilibrium when the transmission coils have no position misalignment. Equation (2) is modified as (3), where I_{m1} is the primary current amplitude.

$$v_{u1A} = L_{1Ys}\frac{di_{u1}}{dt} + M\frac{di_{u2}}{dt} - \omega I_{m1}\left\{M_{c1}\cos\omega t + \left(M_{a1} - M_{b1}\right)\cos\left(\omega t - \frac{2}{3}\pi\right) + \left(M_{a1} - M_{b1}\right)\cos\left(\omega t - \frac{4}{3}\pi\right)\right\} \quad \cdots(3)$$

Equation (3) has three cosine waves with a phase delayed by 120 or 240deg. Thus, the condition for canceling the effect of the cross-coupling is satisfying

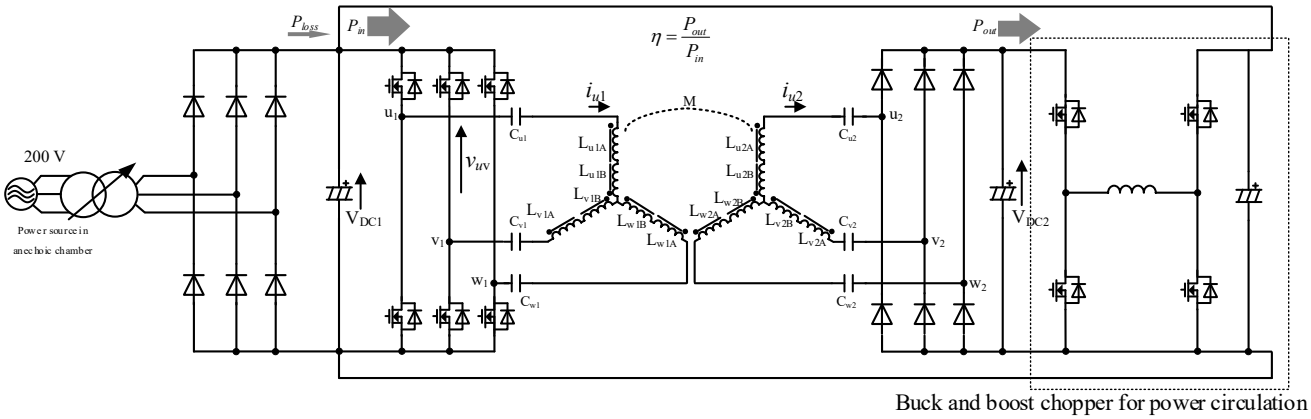

Fig. 4. Circuit configuration of the 22-kW WPT system. The buck and boost chopper is used for power circulation for the test in the anechoic chamber with limited power capacity.

$$M_{a1} = M_{b1} + M_{c1} \quad \text{..... (4).}$$

The cancellation condition is (5) with the coupling coefficients k_{a1}, k_{b1}, and k_{c1} because the self-inductance of the primary coils is common.

$$k_{a1} = k_{b1} + k_{c1} \quad \text{..... (5)}$$

In the same manner, the cancellation condition of the induced voltage on the secondary side is

$$k_{a2} = k_{b2} + k_{c2} \quad \text{..... (6).}$$

By satisfying both (5) and (6), the induced voltage on the L_{u1A} is simplified as

$$v_{u1A} \approx L_{1Ys} \frac{di_{u1}}{dt} + M \frac{di_{u2}}{dt} \quad \text{..... (7).}$$

This is the same as the induced voltage of a single-phase WPT system. It means that the interference among the primary coils and the secondary coils can be canceled by the structure of 12 coils.

Eqs. (5–6) provides the limitation on the figure of transmission coils. In Fig. 1, the coupling k_{an} (n = 1, 2) tends to be the strongest among the cross-coupling because k_{an} is the coupling between the adjacent coils in the same plane. In order to satisfy (5–6), only the coupling k_{bn} and k_{cn} should be improved without increasing the coupling k_{an}. It prevents shrinking the total radius $r + x$ of the transmission coils.

For the prototype, physical parameters of the transmission coils, such as the width, the depth, the thickness, and the distance between the coils, have been determined by cut-and-try with an electromagnetic analysis in this paper. The end of the cut-and-try design is determined by the remaining coupling. The ideal conditions are $k_{an} = k_{bn} + k_{cn}$, as shown in (5–6). From these equations, the remaining magnetic coupling is $k_{an} - k_{bn} - k_{cn}$. The transmission coils are designed so that the remaining coupling $k_{an} - k_{bn} - k_{cn}$ is less than 1/10 of the coupling k ($= M / (L_{1Ys}L_{2Ys})^{0.5}$). Here the coupling k is the main coupling between the primary coils and the secondary coils.

It should be noted that the misalignment of coils and parameter errors on resonance may cause the degradation on the transmission power and efficiency because the cancellation conditions of the cross-coupling, as shown by (5–6), are developed based on the assumption of three-phase equilibrium. Besides, the reduction in radiated emission will not be affected by the misalignment of coils because the cancellation of the radiated emission is satisfied by pairs of coils connected in series with the same current, such as L_{u1A} and L_{u1B}.

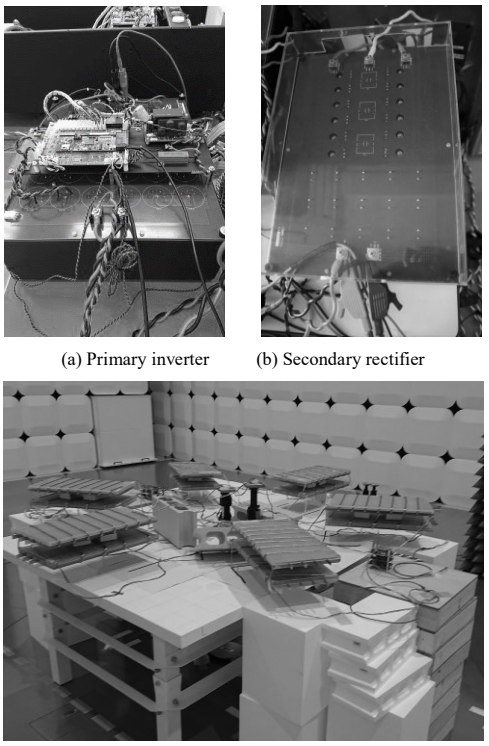

(a) Primary inverter (b) Secondary rectifier

(c) Transmission coils

Fig. 5. The 22-kW prototype.

3. 22-kW Prototype

3.1 System Configuration In this chapter, the 22-kW WPT system is experimentally demonstrated. Figures 4 and 5 show the system configuration and prototype for the evaluation, respectively. The input is connected to the variable transformer to adjust the input DC voltage. Note that a PWM rectifier will be installed instead of the adjustable transformer and diode-bridge rectifier for a product. The prototype has a diode bridge rectifier and bidirectional buck-boost chopper for the test in an anechoic chamber with limited input power.

The bidirectional buck-boost chopper circuit plays a role in circulating power between the output and the input of the system.

Table I. Specification of 22-kW prototype.

Parameters		Symbols	Value	
Input power		P_m	25	kW
Primary voltage at rated power		V_{DC1}	650	V
Secondary voltage		V_{DC2}	200-400	V
Transmission frequency		f	80	kHz
Air gap		g	90	mm
Core width		x	500	mm
Core length		y	250	mm
Core thickness		z	10	mm
Radius		r	750	mm
Number of turns	Primary	N_1	8	turn
	Secondary	N_2	5	turn
Self-inductance	Primary	L_{1Y}	21.8	μH
	Secondary	L_{2Y}	8.52	μH
Main coupling		k	0.55	
Core		TDK, PC95		
Litz wire		2UEWLZ 7×130 (ϕ0.1)		
MOSFETs		ROHM, BSM300D12P2E001		
Diodes		Infineon Technologies, IDW40G120C5BFKSA1		
Deadtime		T_d	500	ns

The secondary DC voltage V_{DC2} is adjustable between 200 to 400 V by the bidirectional buck-boost chopper because it is a typical voltage range of onboard batteries. The AC power source in the anechoic chamber supplies only the power loss in the WPT system and the bidirectional buck-boost chopper due to the configuration.

Figures 5 (c) shows the transmission coils for the 22-kW test. The cross-coupling is k_{a1} = 0.0043, k_{b1} = 0.0026, k_{c1} = 0.0026, k_{a2} = 0.0090, k_{b2} = 0.0013, and k_{c2} = 0.0006. The developed transmission coils satisfy the cross-coupling reduction condition expressed in (5–6). Air gaps between the primary coils and the secondary coils are 90 mm because the physical parameters of the coils are determined by the cut-and-try method in this paper. The proposed configuration is also effective for WPT systems with different air-gap. The air gap does not affect the reduction performance of the radiation noise and cross-coupling. The radiation noise reduction is achieved by the pairs of two coils, placed opposite, on each the primary and the secondary side. Although, the interference reduction condition expressed in (5) and (6) are satisfied on each the primary side and the secondary side, respectively, even if the air gap is changed.

3.2 Parameter Design In this chapter, the design of the 22-kW three-phase WPT system is explained. Table I shows the parameters of the prototype. First, the inductance of coils is designed. The three-phase diode bridge rectifier is represented as an AC resistance. The equivalent AC resistance R_{eq} of the rectifier is (8).

$$R_{eq} = \frac{8}{\pi^2}\frac{\left(V_{DC2}/2\right)^2}{P_m/3} = \frac{6}{\pi^2}\frac{V_{DC2}^2}{P_m} \quad \text{..... (8)}$$

The AC resistance is introduced by expanding the analysis of the equivalent resistance of the single-phase rectifier in (23) with a rated output power P_m and the DC output voltage V_{DC2} on the secondary side. The rated output power is 22 kW with a 400-V of secondary DC voltage. The system has a margin on the output power, considering the power loss in the system. Thus, the equivalent resistance is calculated with V_{DC2} = 400 V and P_m = 25 kW.

Equation (9) is introduced from the impedance matching condition, where ω ($\omega = 2\pi f$) is the angular transmission frequency, and k is the nominal value of the coupling coefficient. The equivalent resistance of the rectifier should be equals to the self-inductance of the secondary coils for the impedance matching. For simplicity, the parasitic resistances of the coils are ignored.

$$L_{2Y} = L_{u2} = L_{v2} = L_{w2} = \frac{6}{\pi^2 k\omega}\frac{V_{DC2}^2}{P_m} \quad \text{..... (9),}$$

Half of the L_{2Y} is the inductance for each coil connected in series on the phase. The primary inductance should be designed from the voltage gain from the primary side to the secondary DC.

From (9), the primary inductance is

$$L_{1Y} = L_{u1} = L_{v1} = L_{w1} = \frac{6}{\pi^2 k\omega}\frac{V_{DC1}^2}{P_m} \quad \text{..... (10).}$$

Then, the resonant capacitors C_{u1}, C_{v1}, C_{w1}, C_{u2}, C_{v2}, and C_{w2} are selected to resonate with the self-inductance of each coil. Series-series compensation[24] is used in this paper. The reactance of the capacitors must be equals to the reactance of the inductance of the coils at the transmission frequency in the series-series compensation.

$$C_{u1} = C_{v1} = C_{w1} = \frac{1}{\omega^2 L_{1Y}},\ C_{u2} = C_{v2} = C_{w2} = \frac{1}{\omega^2 L_{2Y}}$$

..... (11)

For the ZVS operation of the inverter, the operating frequency of the inverter is slightly higher than the resonant frequency, which is determined by (9–11).

4. Experimental Verification of 22-kW Prototype

4.1 Rated Power Test Figure 6 shows the operation waveforms with a 22-kW of the output power, a 650-V of the primary DC voltage V_{DC1}, and a 400-V of the secondary DC voltage V_{DC2}. The bidirectional buck-boost chopper controls the secondary DC voltage to 400 V in order to emulate the onboard battery. The waveform in Fig. 6(a) is the line voltage. The zero-cross of the primary current is synchronized with the voltage rise and fall of the line voltage. It means that the primary inverter operates in the resonant condition. From Fig. 6 (b), it is confirmed that the three-phase primary current is at equilibrium. The output voltage slowly steps up or down by the ZVS operation.

4.2 Efficiency Evaluation The system efficiency of the 22-kW prototype is evaluated. The DC-to-DC efficiency, which is defined as the ratio between the input power and the output power of the DC stage, is measured by the power analyzer (Yokogawa, WT1600). Figure 7 shows the efficiency characteristic of the WPT system. The efficiency indicated in Fig. 7 contains the power loss in the inverter and the diode bridge rectifier. The secondary DC voltage is controlled at 200, 300, 400 V to emulate the constant voltage load, such as an onboard battery. When the battery voltage is lower than 400 V, the output power is derated by the current limit of the secondary coils and diodes. The maximum DC-to-DC efficiency is 91.3% at an output power of 5.0 kW, 91.3% at 10 kW, and 91.1% at 22 kW when the secondary DC voltage is 200, 300, and 400 V.

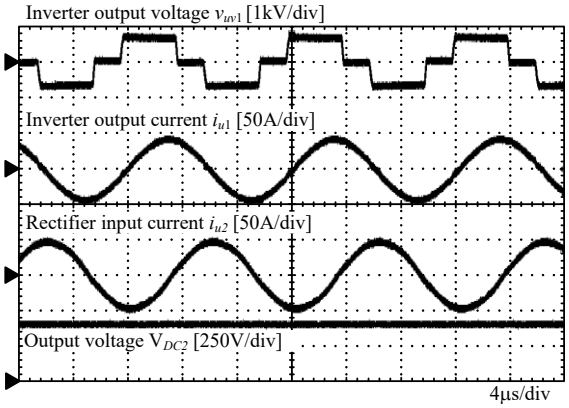

(a) Inverter output voltage, current, rectifier input current and output voltage.

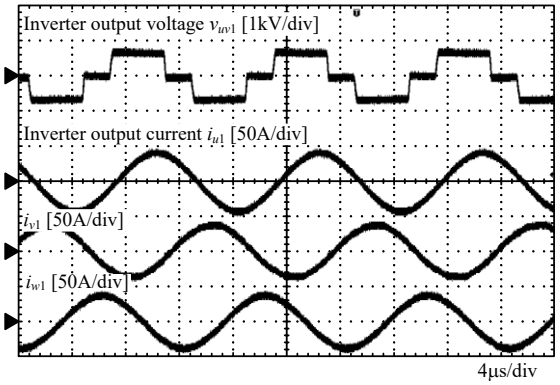

(b) Inverter output voltage and output current on each phase

Fig. 6. Operation waveforms of the proposed three-phase WPT system. The output power is 22 kW, primary DC voltage is 650 V, and secondary DC voltage is 400 V.

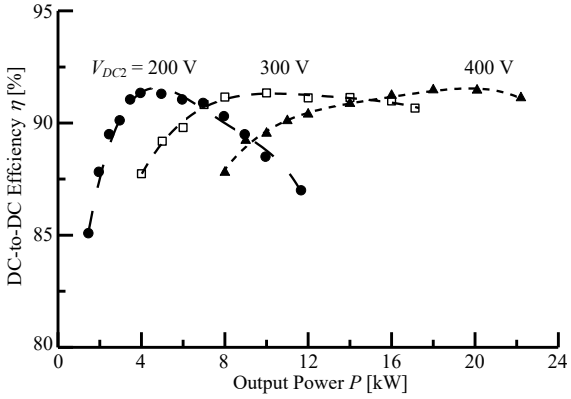

Fig. 7. Efficiency characteristic with different secondary DC voltage.

Figure 8 shows a power loss breakdown of the system when the output power is 22 kW. In this analysis, the primary DC voltage is 650 V, and the DC voltage on the secondary side is 400 V. The total power loss measured by the experiment is 2.16 kW. On the other hand, the sum of the calculated power loss is 1.90 kW. The error between the calculation and the experiment is 260 W, where it is 1.2% of the output power. In other words, the measured efficiency is 91.1%, as against the calculation value of 92.0%.

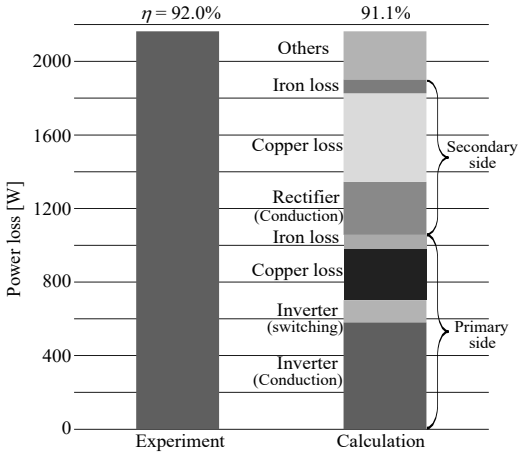

Fig. 8. Breakdown of power loss of 22-kW prototype.

In the calculation, the conduction loss of the MOSFETs dominates the power loss. It accounts for 26.9% of the total loss. The second-largest power loss is the copper loss of the secondary coil because the secondary current I_2 is larger than I_1. It accounts for 22.3% of the total loss.

4.3 Electromagnetic Emission Test for CISPR guidelines The magnetic and electric field is measured in the 10-m anechoic chamber of the Industrial research institute of Niigata prefecture in Niigata, Japan. The measurements are fully compliant with CISPR 11 et. 6.0 published in 2015, and AMD. 1 published in 2016, class A, group 2 (25). Especially, this paper focuses on only the WPT system used in all locations other than those allocated in residential environments. Thus, the WPT system is evaluated with the regulations for class A. The measurement results can be compared with WPT systems, which will be developed from this point of time, with the fair condition because the fairness of the measurement conditions is guaranteed by CISPR 11.

The transmission coils are placed on the turntable and rotated by 360 degrees during the measurement. The highest recorded level of the electromagnetic radiation at each frequency is recorded. The loop antenna (ETS Lindgren, 6502) and Broadband antenna (Teseq, CBL6111D) are used for the measurement of a magnetic field and electric field, respectively. The measurement distance from the edge of the system is 10 m, according to the CISPR 11. The emission with a 22 kW of output power and a 400 V of the secondary DC voltage is measured. Note that the diode bridge rectifier, inverter, high-frequency rectifier, and buck-boost chopper circuit are put in an underground pit in order to evaluate the emission from only the transmission coils.

Figure 9 shows the magnetic field measured in the 10-m anechoic chamber with the peak detection. The line highlighted by gray is the background noise, which is measured even when the WPT system is not operated. The dotted line represents the regulation of CISPR 11, class A, group 2. In the CISPR 11, the regulation on the radiated magnetic field within 150 kHz to 30 MHz has been set up. The regulation on the frequency lower than 150 kHz is under discussion. The magnetic field on the x-axis, y-axis, z-axis at the fundamental frequency is 74.9, 70.1, and 60.9dBμA/m, respectively.

Figure 10 shows the electric field measured in the 10-m anechoic chamber. The line highlighted by gray is the background noise, which is measured even when the WPT system is not operated. The

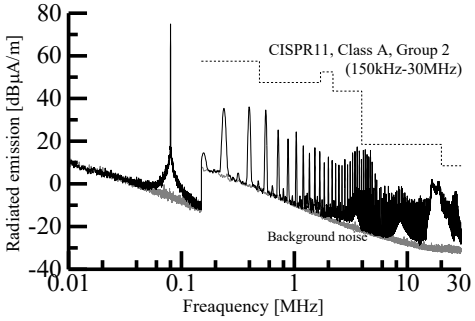

(a) x-axis

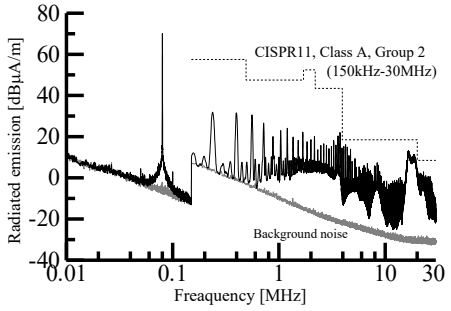

(b) y-axis

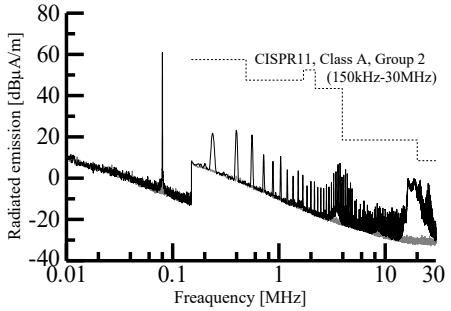

(c) z-axis

Fig. 9. Magnetic field measured in the 10-m anechoic chamber. The measurement is fully compliant with CISPR 11.

dotted line represents the regulation of CISPR 11, class A, group 2. In the CISPR 11, the regulation on the radiated electric field within 30 MHz to 1 GHz has been set up. The electric field of the prototype fully satisfies the regulation of CISPR 11 with a large margin. From the above results, the proposed WPT system fully satisfies the regulation of CISPR 11, class A, group 2.

4.4 Electromagnetic Emission Test for ICNIRP guideline Figure 11 shows the magnetic field strength regarding the distance from the edge of coils and the reference level for general public exposure to time-varying magnetic fields published by ICNIRP in 2010[26]. The radiation noise is measured with ELT-400 (Narda Safety Test Solutions). Note that the measurement has been held in the semi-anechoic chamber with limited area. The measurement result shows that the proposed WPT system complies with the reference levels for general public exposure at 85 kHz published by ICNIRP in 2010 by ensuring a separation distance of 340 mm or more from the edge of the coils.

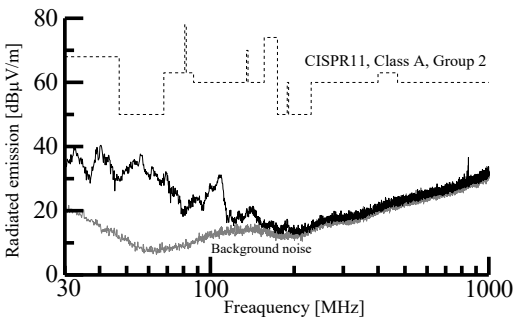

(a) Horizontal polarized wave

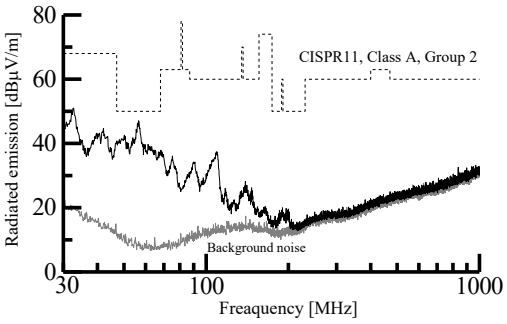

(b) Vertical polarized wave

Fig. 10. Electric field measured in the 10-m anechoic chamber. The measurement is fully compliant with CISPR 11.

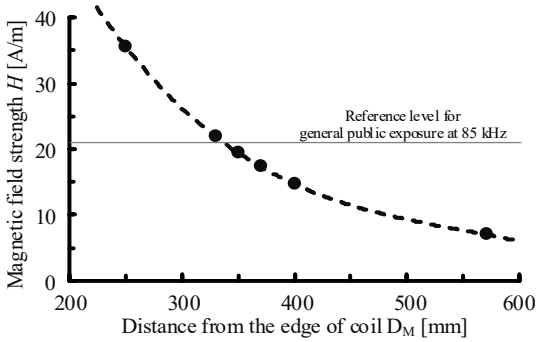

Fig. 11. Magnetic field strength regarding distance from the edge of coil and reference level for general public exposure at 85 kHz published by ICNIRP in 2010.

5. Conclusion

In this paper, the 22-kW three-phase WPT system, which fully complies with CISPR and ICNIRP guidelines without the effect of the cross-coupling is developed and demonstrated. The WPT system transmits power through 12 coils, which are circularly placed every 60 degrees, to reduce electromagnetic emission and cross-coupling effect. The maximum efficiency of the proposed system from the primary DC side to the secondary DC side is 91.1% with an output power of 22 kW and an output voltage of 400 V. Finally, the electromagnetic compatibility of the 22-kW prototype is evaluated in the anechoic chamber according to the measurement method in CISPR 11. The magnetic field and the electric field fully comply with the guideline of CISPR 11, class A, group 2. Besides, the WPT system satisfies the regulation in magnetic field strength regulated by ICNIRP 2010 by ensuring a separation distance of 340

mm or more from the edge of coils.

In future work, the effect of a misalignment and parameter error for resonance on the transmission efficiency and electromagnetic emission will be evaluated.

References

(1) R. Bosshard, J. W. Kolar, J. Mühlethaler, I. Stevanović, B. Wunsch and F. Canales, "Modeling and η–α Pareto Optimization of Inductive Power Transfer Coils for Electric Vehicles," IEEE Journal of Emerging and Selected Topics in Power Electronics, Vol. 3, No. 1, pp. 50-64 (2015)

(2) F. Musavi, M. Edington and W. Eberle, "Wireless power transfer: A survey of EV battery charging technologies," 2012 IEEE Energy Conversion Congress and Exposition (ECCE), pp. 1804-1810 (2012)

(3) S. Li, C. C. Mi, "Wireless Power Transfer for Electric Vehicle Applications," IEEE Journal of Emerging and Selected Topics in Power Electronics, Vol. 3, No. 1, pp. 4-17 (2015)

(4) G. Lovison, T. Imura, H. Fujimoto, Y. Hori, "Secondary-side-only Phase-shifting Voltage Stabilization Control with a Single Converter for WPT Systems with Constant Power Load," IEEJ Journal of Industry Applications, Vol. 8, No. 1, pp. 66-74 (2019)

(5) S. Y. R. Hui, W. Zhong and C. K. Lee, "A Critical Review of Recent Progress in Mid-Range Wireless Power Transfer," IEEE Transactions on Power Electronics, Vol. 29, No. 9, pp. 4500-4511 (2014)

(6) K. Kusaka, K. Furukawa, J. Itoh, "Development of Three-Phase Wireless Power Transfer System with Reduced Radiation Noise," IEEJ Trans. on Industry Applications, Vol. 8, No. 4, pp. 600-607 (2019)

(7) T. Koyama, K. Umetani, E. Hiraki, "Design Optimization Method for the Load Impedance to Maximize the Output Power in Dual Transmitting Resonator Wireless Power Transfer System," IEEJ Journal on Industry Applications, Vol. 7, No. 1, pp. 49-55 (2018)

(8) S. Lee, B. Lee and J. Lee, "A New Design Methodology for a 300-kW, Low Flux Density, Large Air Gap, Online Wireless Power Transfer System," IEEE Trans. on Industry Applications, Vol. 52, No. 5, pp. 4234-4242 (2016)

(9) SAE, "Wireless Power Transfer for Light-Duty Plug-in/Electric Vehicles and Alignment Methodology," The Standard SAE J2954 (2019)

(10) A. Foote and O. C. Onar, "A review of high-power wireless power transfer," 2017 IEEE Transportation Electrification Conference and Expo (ITEC), pp. 234-240 (2017)

(11) A. Ridge, K. K. Ahamad, R. McMahon and J. Miles, "Development of a 50 kW Wireless Power Transfer System," 2019 IEEE PELS Workshop on Emerging Technologies: Wireless Power Transfer (WoW), pp. 406-409 (2019)

(12) J. Tritschler, S. Reichert and B. Goeldi, "A practical investigation of a high power, bidirectional charging system for electric vehicles," 2014 16th European Conference on Power Electronics and Applications, pp. 1-7 (2014)

(13) K. Kusaka, R. Kusui, J. Itoh, D. Sato, S. Obayashi, M. Ishida, "A 22 kW-85 kHz Three-phase Wireless Power Transfer System with 12 coils," 2019 IEEE Energy Conversion Congress & Expo (ECCE), pp. 3340-3347 (2019)

(14) S. Y. Choi, S. Y. Jeong, B. W. Gu, G. C. Lim and C. T. Rim, "Ultraslim S-Type Power Supply Rails for Roadway-Powered Electric Vehicles," IEEE Transactions on Power Electronics, vol. 30, no. 11, pp. 6456-6468 (2015)

(15) H. H. Wu and M. P. Masquelier, "An overview of a 50kW inductive charging system for electric buses," 2015 IEEE Transportation Electrification Conference and Expo (ITEC), pp. 1-4 (2015)

(16) T. Shijo, K. Ogawa, M. Suzuki, Y. Kanekiyo, M. Ishida, S. Obayashi, "EMI Reduction Technology in 85 kHz Band 44 kW Wireless Power Transfer System for Rapid Contactless Charging of Electric Bus", 2016 IEEE Energy Conversion Congress & Expo (ECCE) 2016, No. EC-0641 (2016)

(17) Y. Tanikawa, M. Kato, T. Imura, Y. Hori, "Experiment of magnetic resonant coupling three-phase wireless power transfer," 2013 World Electric Vehicle Symposium and Exhibition (EVS27), pp. 1-8 (2013)

(18) M. Kim, H. Kim, D. Kim, Y. Jeong, H. Park and S. Ahn, "A Three-Phase Wireless-Power-Transfer System for Online Electric Vehicles With Reduction of Leakage Magnetic Fields," IEEE Trans. on Microwave Theory and Techniques, Vol. 63, No. 11, pp. 3806-3813 (2015)

(19) C. Song, H. Kim, D. H. Jung, K. Yoon, Y. Cho, S. Kong, Y. Kwack, J. Kim, "Three-phase magnetic field design for low EMI and EMF automated resonant wireless power transfer charger for UAV," 2015 IEEE Wireless Power Transfer Conference (WPTC), pp. 1-4 (2015)

(20) K. Liu, F. C. Y. Lee, "Zero-voltage switching technique in DC/DC converters," IEEE Trans. on Power Electronics, Vol. 5, No. 3, pp. 293-304 (1990)

(21) Y. Tanikawa, M. Kato, T. Imura and Y. Hori, "Experiment of magnetic resonant coupling three-phase wireless power transfer," 2013 World Electric Vehicle Symposium and Exhibition (EVS27), pp. 1-8 (2013)

(22) J. Kim, H. C. Son, D. H. Kim and Y. J. Park, "Impedance matching considering cross coupling for wireless power transfer to multiple receivers," 2013 IEEE Wireless Power Transfer (WPT), pp. 226-229 (2013)

(23) R. L. Steigerwald, "A Comparison of Half-Bridge Resonant Converter Topologies," IEEE Trans. on Power Electronics, Vol. 3, No. 2, pp. 174-182 (1988)

(24) Y. H. Sohn, B. H. Choi, E. S. Lee, G. C. Lim, G. Cho, C. T. Rim, "General Unified Analyses of Two-Capacitor Inductive Power Transfer Systems: Equivalence of Current-Source SS and SP Compensations," IEEE Trans. on Power Electronics, Vol. 30, No. 11, pp. 6030-6045 (2015)

(25) Comité international spécial des perturbations radioélectriques (CISPR), "Industrial, scientific and medical equipment - Radio-frequency disturbance characteristics - Limits and methods of measurement," CISPR 11, Ed. 6.2 (2019)

(26) ICNIRP, "ICNIRP guidelines for limiting exposure to time-varying electric and magnetic fields (1 Hz to 100 kHz)," Health physics, Vol. 99, No. 6, pp. 818-836 (2010)

Keisuke Kusaka (Member) received his B.S. and M.S. degrees in electrical, electronics and information engineering from Nagaoka University of Technology, Niigata, Japan in 2011, 2013, respectively. From 2015 to 2016, he was with Swiss Federal Institute of Technology in Lausanne (EPFL), Switzerland as a Trainee. In 2016, he received his Ph.D. degree in energy and environment science from Nagaoka University of Technology. He had been with Nagaoka University of Technology, Niigata, Japan as a researcher from 2016 to 2018, and an assistant professor from 2018 to 2021. He is currently a tenure track lecturer at the same university. His current research interests include the areas of inductive power transfer systems and high-frequency converters. Dr. Keisuke is a member of the Institute of Electrical Engineers of Japan and Society of Automotive Engineers of Japan. He received the second prize paper award in IPEC-Niigata 2018.

Rintaro Kusui (Student-member) was received his B.S. degree in electrical, electronics and information engineering from Nagaoka University of Technology, Niigata, Japan in 2020. Presently, he is a Ph.D. candidate at Nagaoka University of Technology, Niigata, Japan. He is the student member of IEEJ and IEEE.

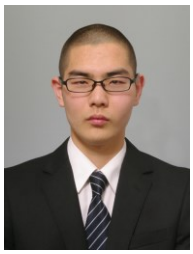

Jun-ichi Itoh (Senior-member) was born in Tokyo, Japan, in 1972. He received his M.S. and Ph.D. degree in electrical and electronic systems engineering from Nagaoka University of Technology, Niigata, Japan in 1996, 2000, respectively. From 1996 to 2004, he was with Fuji Electric Corporate Research and Development Ltd., Tokyo, Japan. He was with Nagaoka University of Technology, Niigata, Japan as an associate professor. Since 2017, he has been a professor. His research interests are matrix converters, dc/dc converters, power factor correction techniques, energy storage system and adjustable speed drive systems. He received IEEJ Academic Promotion Award (IEEJ Technical Development Award) in 2007. In addition, he also received Isao Takahashi Power Electronics Award in

IPEC-Sapporo 2010 from IEEJ, 58th OHM Technology Award from The Foundation for Electrical Science and Engineering, November, 2011, Intelligent Cosmos Award from Intelligent Cosmos Foundation for the Promotion of Science, May, 2012, and Third prize award from Energy Conversion Congress and Exposition-Asia, June, 2013. Prizes for Science and Technology (Development Category) from the Commendation for Science and Technology by the Minister of Education, Culture, Sports, Science and Technology, April 2017. Dr. Itoh is a senior member of the Institute of Electrical Engineers of Japan, the Society of Automotive Engineers of Japan and the IEEE.

Daisuke Sato (Member) was born in Hokkaido, Japan, in 1989. He received his B.S. and M.S. degrees in 2012, 2014, respectively in electrical, electronics and information engineering from Nagaoka University of Technology, Nagaoka, Japan. In 2017, he received his Ph.D. degree in energy and environment science from Nagaoka University of Technology. In 2017, he launched Nagaoka Motor Development Co., Ltd. as a co-founder. He is currently CEO.

Tetsu Shijo (non-member) received B.S. M.S., and Ph.D. degrees from Tokyo Institute of Technology, Tokyo, Japan in 2002, 2004, and 2007, respectively. From 2007, he is with Toshiba Corporation.

Shuichi Obayashi (non-member) received his degree in Master of Engineering from Kyoto University, Kyoto, Japan in 1987. From 1987, he is with Toshiba Corporation.

Masaaki Ishida (non-member) received his B.S. degree from Keio University, Tokyo, Japan in 1987. From 1987, he is with Toshiba Corporation.